J Solid State Electrochem (2015) 19:485–495
DOI 10.1007/s10008-014-2621-x

ORIGINAL PAPER

Electrochemical dissolution behaviour of Ti90Al6V4 and Ti60Al40 used for ECM applications

Martin Weinmann · Moritz Stolpe · Olivier Weber · Ralf Busch · Harald Natter

Received: 9 May 2014 / Revised: 21 August 2014 / Accepted: 23 August 2014 / Published online: 5 September 2014

Abstract The dissolution behaviour of two different titanium alloys in aqueous electrolytes has been investigated. Therefore, a commercial titanium grade 5 (Ti90Al6V4) alloy and a self-produced Ti60Al40 alloy were compared. After preparation by arc melting and a heat treatment, an extensive characterization of the alloy by X-ray diffraction and energy-dispersive X-ray spectroscopy has been performed. The electrochemical behaviour of the alloys in different electrolytes was investigated using different techniques like linear sweep voltammetry and electrochemical impedance spectroscopy. An influence of the electrolyte composition and the titanium content of the alloy on the dissolution process could be observed. Higher titanium content of the alloy impedes the dissolution process. An increase of chloride ions in the electrolyte facilitates the dissolution. The results could be proved by an electrochemical machining (ECM) process in lab scale.

Keywords Electrochemical machining · Electrochemical dissolution · Titanium alloys · Intermetallics

M. Weinmann · H. Natter (✉)
Physical Chemistry, Saarland University, Campus Geb. B2 2, 66123 Saarbrücken, Germany
e-mail: h.natter@mx.uni-saarland.de

M. Stolpe · R. Busch
Metallic Materials, Saarland University, Campus Geb. C6 3, 66123 Saarbrücken, Germany

O. Weber
Production Engineering, Saarland University, Campus Geb. A4 2, 66123 Saarbrücken, Germany

O. Weber
Center for Mechatronics and Automatization, Gewerbepark Eschberger Weg, Geb. 9, 66121 Saarbrücken, Germany

Introduction

Because of their outstanding material properties, like corrosion stability, high strength-to-density ratio and biocompatibility, titanium and its alloys are promising materials for different applications. The main focus of this paper is on titanium-aluminium alloys which are used in many fields of application. Ti90Al6V4 (titanium grade 5) is a widespread material used for many medical applications and implants [1–3] whereas titanium aluminides (intermetallic phase with various Al contents), e.g. Ti60Al40, are often used in aerospace applications [4, 5] as a replacement for iron- and nickel-based alloys. Due to the high mechanical strength [5–7], conventional machining like drilling, turning or milling is not suitable for manufacturing structures of small dimensions. Additionally, the surface quality is not sufficient by using these techniques [8]. Therefore, another process for machining of these materials has to be introduced.

A promising technique is the so-called electrochemical machining (ECM)—an electrochemical dissolution process that creates very smooth surfaces with a high precision and without limitations to the mechanical properties of the metallic alloys [9]. Nowadays, ECM is gaining more and more importance for the production of sophisticated parts in high amounts.

In contrast to the other techniques, there is no mechanical and no heat influence on the surface of the machined parts. Therefore, negative factors like initial points for cracks and internal stresses are not initialized by the ECM process. This technique exhibits a very cost-effective production method, allowing the production of a high quality surface in only one production step.

There are different fields of application for the ECM technique in industries. Beside the application in aircraft industry, also the medical field offers many possibilities. In this area, titanium alloys are often used as materials for implants due to

their high biocompatibility [10]. For this reason, many investigations on the corrosion behaviour of Ti90Al6V4 in biological environments and comprehensive investigations on the corrosion behaviour in the medical field are published [11, 12]. Some of these results can be used as an indicator for the dissolution behaviour in the ECM process. Ti60Al40 is a promising material for light-weight constructions, but unfortunately, little is known about the electrochemical dissolution behaviour.

The main problem during the ECM process for titanium and its alloys is the formation of a dense oxide passive layer which inhibits the dissolution process. Without the knowledge of the appropriate processing parameters, an industrial application is impossible. So there has to be chosen a suitable electrolyte and corresponding current parameters. According to the technical importance of Ti60Al40 and Ti90Al6V4, we choose these two materials for a detailed investigation.

In this study, the electrochemical behaviour of titanium alloys was investigated using different techniques like linear sweep voltammetry (LSV) and electrochemical impedance spectroscopy (EIS).

Experimental

Two different kinds of titanium alloys were investigated. On the one hand, a commercial Ti90Al6V4 alloy (Gustoc-Titanbau GmbH, Solingen, Germany) was used and on the other hand, a Ti60Al40 alloy was self-made by arc melting in an argon atmosphere. Titanium rod (E. Wagener GmbH, Neuhausen, Germany) and aluminium pellets (Merck Schuchardt OHG, Hohenbrunn, Germany) were used as basic materials for the alloy preparation. Ingots of the Ti60Al40 alloy were prepared by arc melting the elemental metals under a Ti-gettered, high-purity argon atmosphere. Each ingot was flipped and remelted ten times to ensure homogeneity. Subsequently, rods of the alloy were produced by remelting the ingots under a Ti-gettered, high-purity argon atmosphere using an electrical arc (Edmund Bühler GmbH, Hechingen, Germany) and put the melt by gravity casting into a water-cooled copper mould with a diameter of 15 mm. After casting to a rod of 15-mm diameter, the samples were heat treated in vacuum. The heating rate in a tube furnace was 5 K min^{-1}. Reaching 1,200 °C, the sample was annealed for 40 h at this temperature and cooled down to room temperature during 12 h. After annealing, the rod was cut in discs of 5.2-mm thickness and 12.45-mm diameter by wire-electro discharge machining. After this, they were mechanically polished down to a surface roughness of 6 μm. The structure of all samples used in this study was characterized by X-ray diffraction (XRD) and scanning electron microscopy (SEM). The chemical composition was determined by inductively coupled plasma optical emission spectrometry analysis (ICP-OES) using a Varian 720-ES setup (Varian Inc., Palo Alto, USA) and by energy-dispersive X-ray spectroscopy (EDX). For the XRD measurements, a PANalytical X'Pert Pro diffractometer (PANalytical B.V., Almelo, The Netherlands) with secondary monochromated Cu Kα1/α2 radiation was used. The determination of all crystallographic values (lattice constants, space group and Miller indices) was done by Rietveld refinement using the software Topas (Bruker AXS, Karlsruhe, Germany). The SEM investigations were performed with a JEOL microscope JSM-7000 F (JEOL Ltd., Tokyo, Japan).

Electrochemical measurements were performed in a modified micro-flow cell [13] with a three-electrode setup and a BioLogic SP150 potentiostat (BioLogic SAS, Claix, France). As counter electrode, a platinum wire was used; the reference electrode was Hg/Hg_2SO_4 in 0.5 M sulphuric acid. The ECM measurements were performed in a flow cell (in the following, the term macro-flow cell is used) with a gap between counter electrode and sample of 100 μm and an electrolyte flow of 0.6 L min^{-1} connected to a BOP 20-50 MG potentiostat (Kepco Inc., Flushing, USA) with internal reference. A stainless steel cylinder with a diameter of 12.8 mm was used as counter electrode. Data were acquired using self-programmed LabVIEW software. A schematic view of flow cells used in this work is shown in Fig. 1.

Linear sweep voltammetry and electrochemical impedance spectroscopy were used for the investigation of the dissolution process. The results were analysed using the software EC-Lab from BioLogic.

Results and discussion

Chemical and structural sample characterization

For all samples, the homogeneity, the composition and the structure were analysed by spectroscopic techniques, chemical analysis and X-ray diffraction. The homogeneity of the alloys was measured by EDX line scans which were cross-like arranged over the sample surface with a length of 3.5 mm. The vertical line scans are shown on the left side and the horizontal line scans are shown on the right side of Fig. 2. The elements are marked in different colours. For both alloys, the element distribution is constant over the whole measuring area. Neither precipitations nor decompositions can be observed.

The ICP-OES analysis was used for the quantitative analysis of the sample composition. Both samples were dissolved in a mixture (2.4:1) of HCl (37 wt%)/H_2O_2 (33 wt%) and heated at 120 °C for 4 h under reflux. The resulting solution was diluted with 1 % HNO_3. The results of the analysis are summarized in Table 1. The chemical analysis of the self-prepared sample confirms that the amount of educts used for the preparation of the alloy was also found in the as-prepared

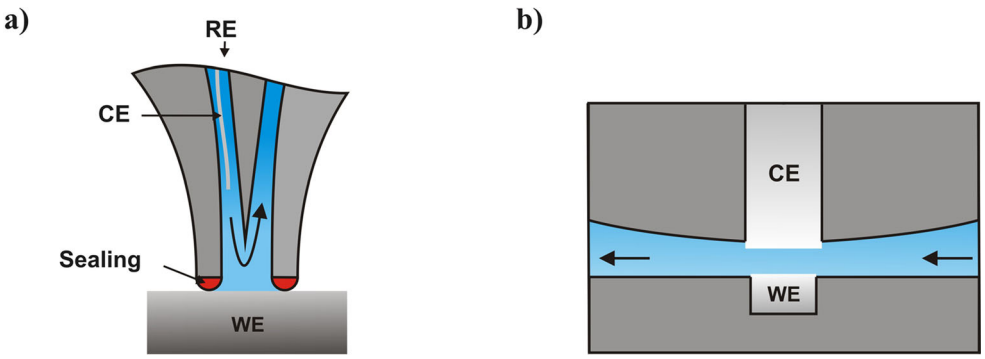

Fig. 1 Schematic view of a micro- (a) and macro-flow cell (b) used for the electrochemical measurements

sample. The chemical composition of the commercial sample corresponds to the manufacturer's data.

The crystallographic structure of the commercial Ti90Al6V4 and the self-made Ti60Al40 sample were measured by X-ray diffraction. Figure 3 shows the corresponding diffraction pattern. The Ti90Al6V4 alloy is a mixture of titanium's cubic α- and hexagonal β-phases [5] which are stabilized by the alloying additives aluminium and vanadium. The Al additive stabilizes the α-phase and vanadium the β-phase. The peak analysis of the diffraction pattern shows that both phases are present. Table 2 summarizes the key data.

The small additive amounts of aluminium and vanadium which are segregated in the grain boundaries cannot be detected by X-ray diffraction. Only a few peaks with very low intensities can be observed. A phase ratio of 1.4 (cubic/hexagonal) can be estimated from the peak intensities (Fig. 3a) at 38.545 and 40.410° (2Θ).

The diffraction pattern of the self-made Ti60Al40 alloy is shown in Fig. 3b. The structure was characterized by Rietveld analysis using the software Topas. A well-fitting result could be received with a tetragonal structure P4/mmm with an *a* and *b* lattice parameter of 3.98985 Å and a *c* lattice parameter of 4.07867 Å. This result corresponds to the estimated phase according to the phase diagram of titanium-aluminium [16].

Electrochemical characterization

EIS studies and modelling of the native oxide layer

It is known that aluminium as well as titanium has in the as-prepared state an oxide layer which protects the materials against dissolution. If they are dissolved, there is always a transpassive dissolution process [17]. One aim of the present work is the investigation of the dissolution behaviour of the two titanium materials in different electrolytes. For this reason, it is important to know the structure and stability of the oxide layers. In the first step, we characterize the native oxide

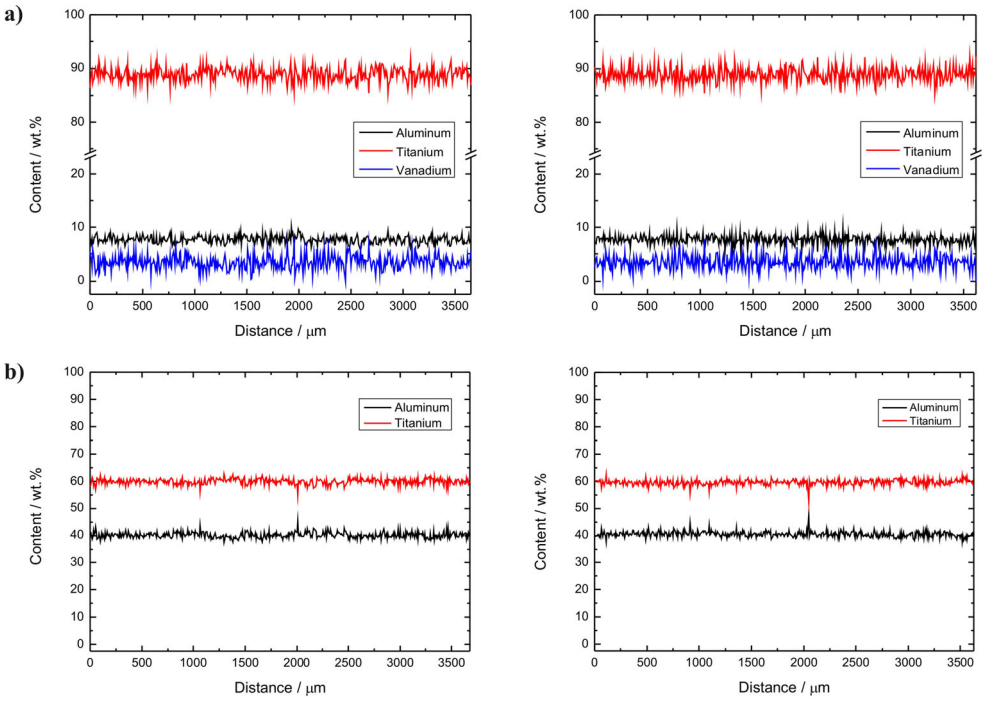

Fig. 2 EDX line scans of Ti90Al6V4 (a) and Ti60Al40 (b) in vertical (*left*) and horizontal (*right*) direction show a homogeneous element distribution

Table 1 Chemical composition of the used samples determined by ICP-OES

Sample	Ti content/wt%	Al content/wt%	V content/wt%
Ti90Al6V4	89	7	4
Ti60Al40	59	41	–

Table 2 Space group and lattice parameters of α- and β-titanium

Phase	Space group	*a*/Å	*b*/Å	*c*/Å	pdf number
α-Ti	P63/mmc	2.9500	2.9500	4.6860	005-0682 [14]
β-Ti	lm3m	3.3065	3.3065	3.3065	044-1288 [15]

layers on both materials by EIS studies. From the evaluation model used for the EIS studies, we get the information which is a combination of layer thickness, porosity and uniformity [18]. Linear sweep voltammetry studies were performed to support the results of the EIS studies. In these experiments, the samples were measured in native state and after different pre-treatments: etching with diluted hydrofluoric acid and additional oxidization in concentrated nitric acid or by an electrochemical step in the corresponding electrolyte.

The literature reports about different kinds of oxide layers on titanium and its alloys which were investigated by impedance spectroscopy [12, 18–21]. There are two main models: The two-layer model of Pan et al. [18] bases on an inner barrier layer and an outer porous oxide layer located on the top of the alloy substrate. A single-layer model was developed by González et al. [12] which assumes only one dense oxide layer on top of the bulk alloy material.

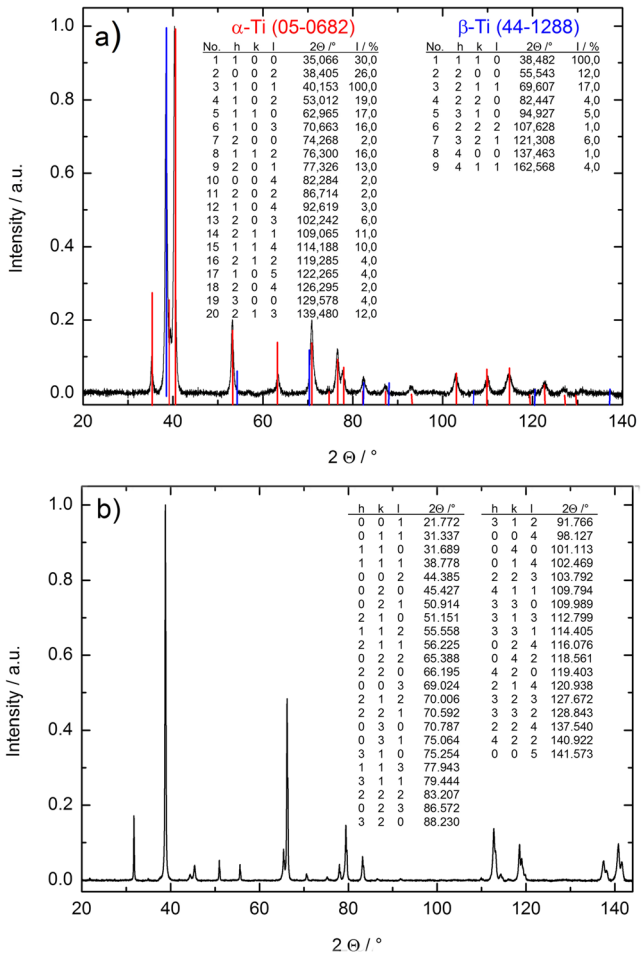

Fig. 3 Background corrected diffraction patterns of Ti90Al6V4 (a) as received and Ti60Al40 (b) after heat treatment. The *inlays* show hkl values and peak positions

For characterization of the native oxide layer, we perform EIS measurements at open circuit potential in a 1 M NaCl solution. The corresponding Nyquist plots are shown in Fig. 4.

The data evaluation according to the single-layer model by González [12] was done with the following equivalent circuit including a constant phase element (CPE) and two resistances R_s and R_b (Fig. 5).

R_s represents the ohmic resistance of the electrolyte and the outer environment. The oxide layer was modelled by a resistance R_b and a CPE Q_b. The impedance $Z(f)$ for a given frequency f of a CPE is given by Eq. 1 [22].

$$Z(f) = \frac{1}{Q(j\cdot\pi\cdot f)^n} \tag{1}$$

where Q and n are model parameter and $j^2=-1$. In the case of $n=1$, the CPE corresponds to a conventional capacitor.

Electrochemical impedance spectroscopy was performed for each material at the corresponding open circuit potential listed in Table 3. The pH value was adjusted to 7.0 and the temperature kept constant at 25 °C. Resulting Nyquist plots are shown in Fig. 4. The data were evaluated using the equivalent circuits mentioned above with the fitting software ZFit (BioLogic SAS, Claix, France). The calculated fitting curves based on the determined parameters (Table 3) are also shown in Fig. 4 (solid lines).

The oxide layer of our sample was represented by the layer resistance R_b and by n. The parameters calculated from the CPEs are associated with the layer thickness and a non-uniform current distribution due to defects and porosity inside the layer. An n value of 1 means a bulk layer without any porosity, and in the absence of a porous layer, the n value is 0.

An analysis of the fit parameter in Table 3 shows that with increasing titanium content, the resistance of the barrier layer R_b increases. This indicates an increase of the oxide layer thickness and its stability. A major stability of oxide film structure which leads to a higher passivity of the surface can be assumed. Investigating the n values, we can see that they are closer to 1 for higher titanium contents. The n value contains information about the layer thickness, porosity and

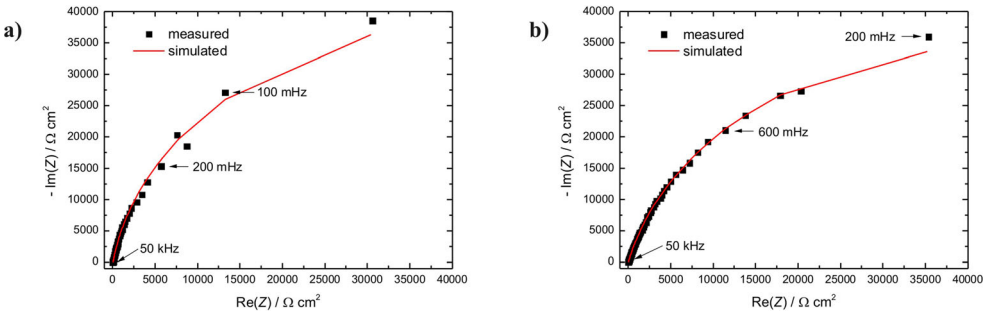

Fig. 4 Nyquist plot of Ti90Al6V4 (**a**) and Ti60Al40 (**b**) at E_{OCP} in 1 M NaCl solution

also the uniformity. So we can expect thicker, more uniform, more homogenous and denser oxide layers for higher titanium contents. These results give a hint to a better solubility of the Ti60Al40 alloy in contrast to the Ti90Al6V4 alloy. Summarizing the EIS results, we conclude that a native oxide layer exists on the surface of both alloys but with different structures. The Ti90Al6V4 alloy has a more stable oxide layer than the Ti60Al40 alloy.

Influence of the oxide layer on the dissolution behaviour of the alloys

In this series of measurements, the influence of the native oxide layer on the electrochemical dissolution behaviour of the both alloys was investigated by linear sweep voltammetry. The experiments were performed in a potential range from −2.0 to +1.0 V (vs. Hg/Hg_2SO_4) in 1 M NaCl, 1 M $NaNO_3$ and 1 M $NaClO_3$ solution. The electrolyte is unstirred. The scan rate was kept constant at 20 mV s^{-1} at pH 7 and at room temperature. The experimental data are displayed in Fig. 6. The corresponding open circuit potential (E_{OCP}) which corresponds to the dissolution resistance is shown in Table 4.

EIS measurements in "Electrochemical characterization" section show that an oxide layer is present in the native state. This oxide layer influences the electrochemical dissolution of the alloys. If the oxide layer is removed by a chemical treatment, the dissolution of the alloy will be accelerated. This can be observed by a negative shift of the E_{OCP}. In contrast to a removal of the oxide layer, a further increase of the oxide layer thickness by oxidation will shift the E_{OCP} value to more positive values. In the first experiment, the alloys were measured in the native state. After these experiments, the oxide layer was influenced by two different ways:

1. The native oxide layer was removed by etching the sample for 10 s in diluted hydrofluoric acid (15 %).
2. The oxide layer thickness was increased by oxidation.

The corresponding E_{OCP} values for the different treatments are shown in Table 4. It can be seen that for each alloy and each electrolyte, there is an influence of the pre-treatment on the E_{OCP}. The thicker the resulting oxide layer, the more positive is the E_{OCP}.

Additionally, the resulting anodic current densities show a dependence of the pre-treatment. Some electrolytes can only dissolve the titanium alloys in an active way by using an HF etching before the dissolution process. Evaluating the measurements of Ti90Al6V4, the curves can be divided in two different regions. Between −1 and 0 V (vs Hg/Hg_2SO_4), an active dissolution was observed (region 1), and for higher potentials (region 2), an oxide layer formation takes place (see Fig. 7).

The current in region 2 results from the oxide layer formation on the unoxidized titanium surface and should correlate with the oxidation power of the electrolyte. It can be seen that the current density in region 2 increases in the order sodium chloride—sodium nitrate—sodium chlorate. Nitrate and chloride ions have a low oxidation power whereas the chlorate ion is a strong oxidation agent.

For Ti60Al40, the chloride electrolyte shows a different behaviour (see Fig. 8). Starting from −0.25 V (vs Hg/Hg_2SO_4), the current density increases very strong without any trend to passivation. For this reason, we assume an active dissolution. The nitrate electrolyte exhibits a similar behaviour like Ti90Al6V4 with the mentioned two regions. The course of the measurement with the chlorate electrolyte cannot clearly be divided in two regions. The current density for anodic potentials is much higher than for the experiment with the nitrate electrolyte indicating a mixture between oxide layer formation and transpassive dissolution. Maybe, a decomposition of chlorate ions takes place which contributes to the resulting current. A hint for this assumption is the step at +

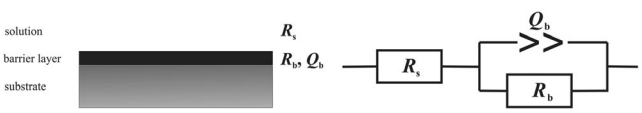

Fig. 5 Single-layer model (*left*) and corresponding equivalent circuit (*right*) used for the evaluation of the EIS data

Table 3 Fitting results for EIS measurements on Ti90Al6V4 and Ti60Al40

Alloy	Electrolyte	R_s/Ω cm^2	Q_b/μFs$^{(n-1)}$cm^{-2}	n value	R_b/MΩ cm^2	E_{OCP}/mV (vs Hg/Hg_2SO_4)
Ti90Al6V4	1 M NaCl	1,468	1.478	0.91	2.8	−841
Ti60Al40	1 M NaCl	485	0.374	0.86	2.7	−986

0.570 V (vs Hg/Hg_2SO_4) which could correspond to the perchlorate formation at +0.512 V (vs Hg/Hg_2SO_4).

The influence of the oxidation power of the used anions was measured by a time resolved recording of the E_{OCP}. The results are given in Fig. 9. An etched sample of Ti90Al6V4 was immersed in the respective electrolyte and E_{OCP} was recorded for 30 min.

The time-dependent evolution of the E_{OCP} values ends in a kind of steady state which depends on the type of electrolyte. The increase of E_{OCP} indicates the formation of an oxide layer. To quantify this process, we regard the potential difference between the initial potential at t=0 s and the potential in the steady state region. From these measurements, we conclude that the

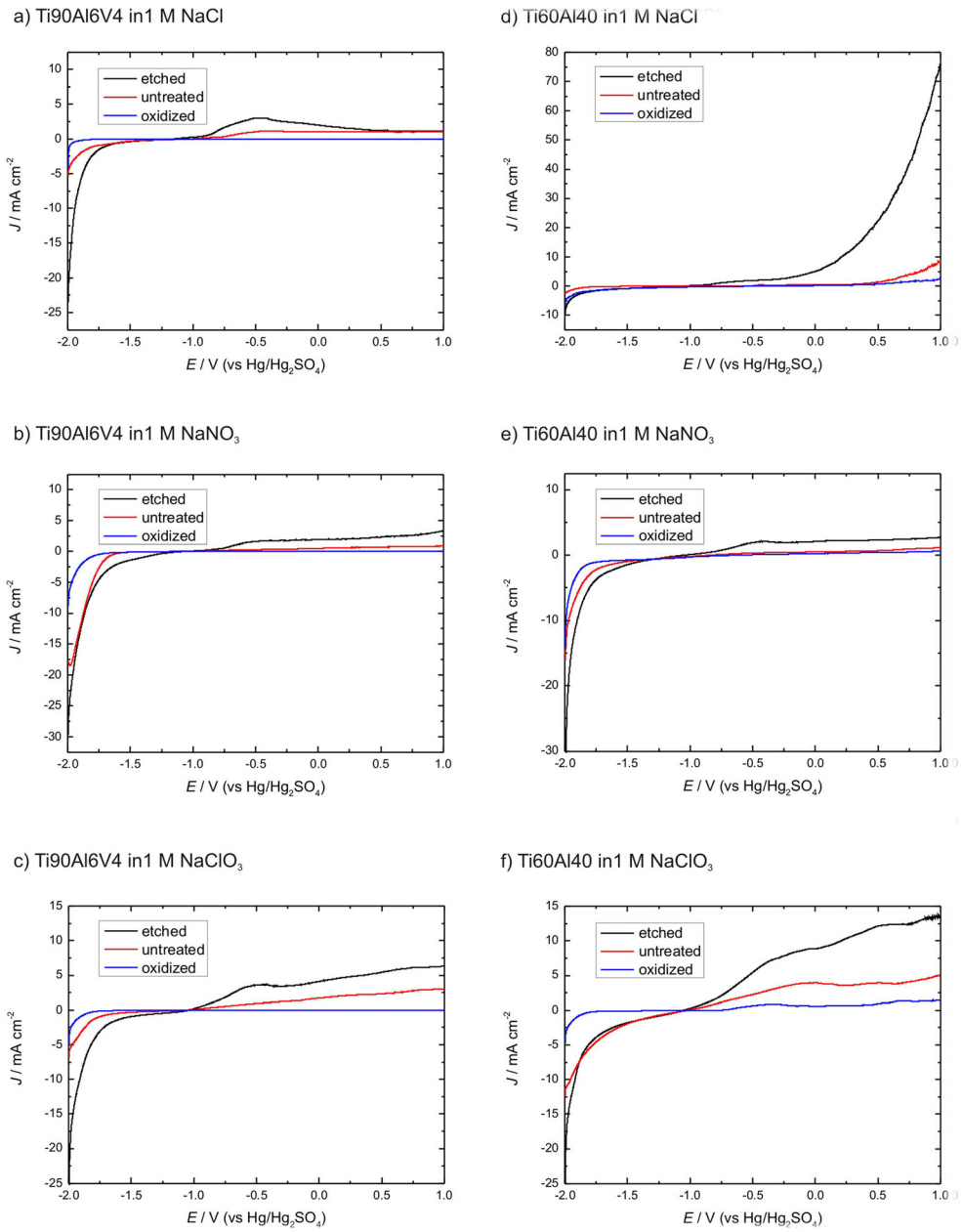

Fig. 6 Linear sweep voltammetry measurements with a scan rate of 20 mV s^{-1} on titanium alloys in different electrolytes

Table 4 Determination of E_{OCP} in different electrolytes

Alloy	Electrolyte	Pre-treatment	E_{OCP}/mV (vs Hg/Hg_2SO_4)
Ti90Al6V4	1 M NaCl	Etched	−897
		Native	−841
		Oxidized	−751
Ti90Al6V4	1 M $NaNO_3$	Etched	−867
		Native	−830
		Oxidized	−670
Ti90Al6V4	1 M $NaClO_3$	Etched	−865
		Native	−799
		Oxidized	−430
Ti60Al40	1 M NaCl	Etched	−1,051
		Native	−986
		Oxidized	−840
Ti60Al40	1 M $NaNO_3$	Etched	−1,020
		Native	−876
		Oxidized	−818
Ti60Al40	1 M $NaClO_3$	Etched	−950
		Native	−852
		Oxidized	−760

formation of an oxide layer is much faster in a chlorate electrolyte than in chloride or nitrate electrolyte.

Dissolution behaviour in an ECM-like process

The experimental proof of the developed model was done by an ECM-like process on the lab scale. Therefore, macro-flow cell experiments were performed. As described in "Experimental" section, it consists of a two-electrode setup with a stainless steel counter electrode and a titanium-alloy working electrode. In this two-electrode setup, the electrodes were directly connected to a power supply. To determine the starting voltage for the material dissolution, the applied

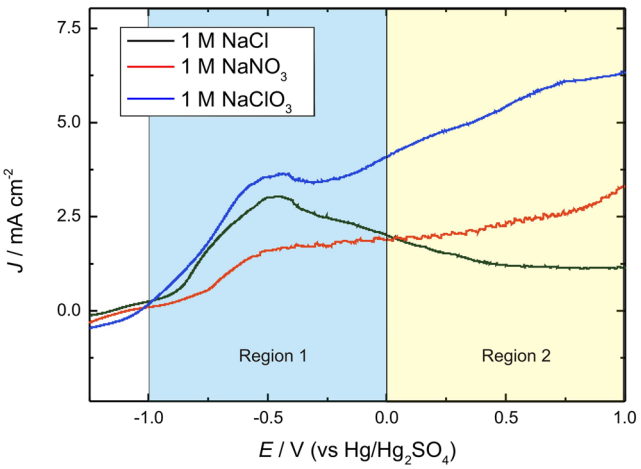

Fig. 7 Dissolution behaviour of etched Ti90Al6V4 samples in different electrolytes (scan rate 20 mV s^{-1})

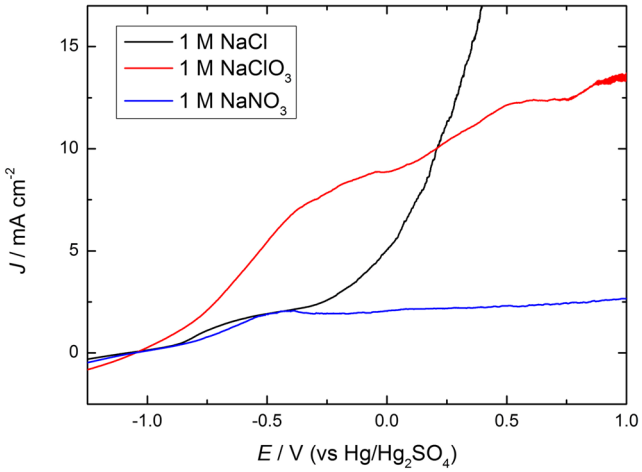

Fig. 8 Dissolution behaviour of etched Ti60Al40 samples in different electrolytes (scan rate 20 mV s^{-1})

voltage was increased from −2 to 10 V with a scan rate of 50 mV s^{-1}. The samples were measured in native state. The resulting current density-time curves can be seen in Fig. 10.

Figure 10 shows that the alloy compositions as well as the electrolyte influence the dissolution behaviour of the material. It is well known that there is a natural oxide layer on top of the titanium alloys. This oxide layer could be verified by electrochemical methods (see "Electrochemical characterization" section). As expected, the current-voltage curves show in both cases a distinct area of passivation. For untreated samples, there is almost no active dissolution but only a transpassive one which starts at the dissolution voltage (E_{diss}). In Fig. 10, E_{diss} can be determined by evaluating the inflection point of the current-voltage curve. E_{diss} is much higher for the titanium rich alloy than for Ti60Al40. The higher the titanium content, the lower the current density during the dissolution process. So it is easier to machine alloys with lower titanium contents.

There is a second influencing factor on the dissolution behaviour. The electrolyte also plays an important role. Compared to the $NaNO_3$ electrolyte, the NaCl electrolyte

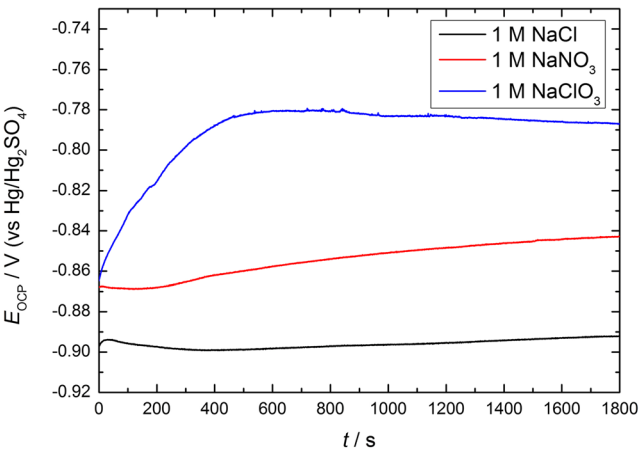

Fig. 9 Time dependence of the E_{OCP} for Ti90Al6V4 measured in different electrolytes

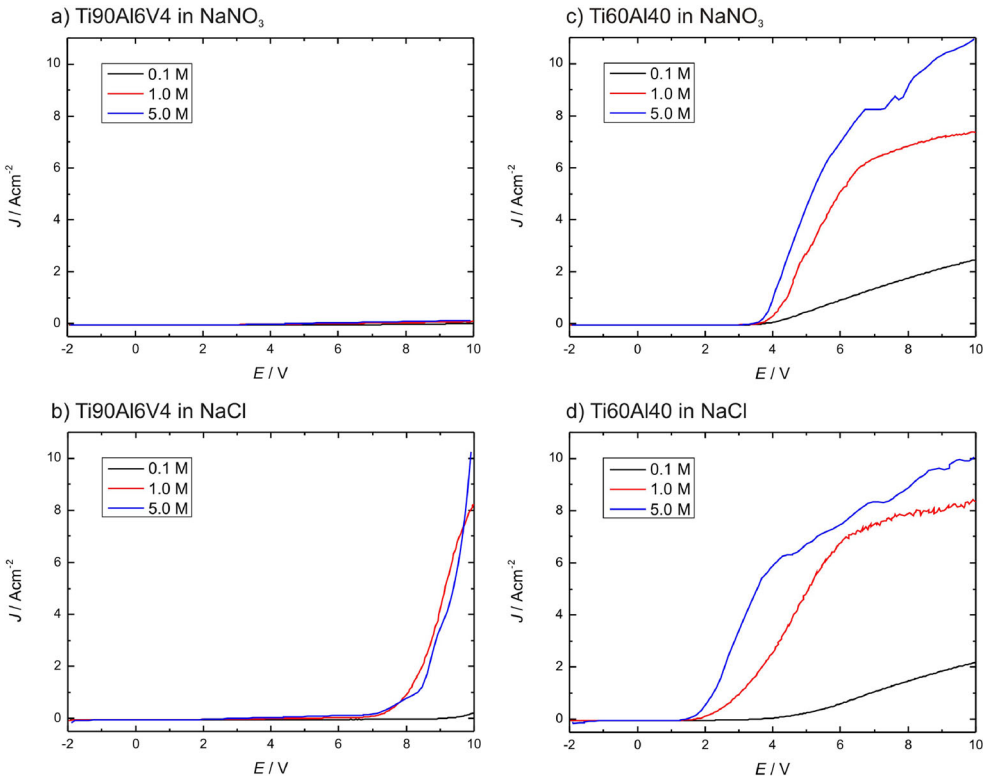

Fig. 10 Determination of starting voltage for dissolution of **a** Ti90Al6V4 and **b** Ti60Al40 in different electrolytes (scan rate 50 mV s^{-1})

lowers E_{diss}: The dissolution starts at lower voltages, which indicates a better machinability using this kind of electrolyte.

As Fig. 10a shows, there is no dissolution for the Ti90Al6V4 alloy using the nitrate electrolyte in the measured voltage range. There is only a passivation of the surface. In the case of halide electrolytes, different dissolution mechanisms [12, 23, 24] were proposed. The difference between these mechanisms is the modification of the formed titanium oxide which is in one case TiO_2 [12, 24] and in the other Ti_2O_3 [23]. The intermediate compounds are the corresponding halide complexes or the protolysis products of the titanium halides. For this reason, kinetic and also thermodynamic effects are responsible for the faster dissolution of the titanium alloys in halide solutions. Therefore, a chloride containing electrolyte could be used for this purpose.

The electrolytes concentration is also very important for the dissolution behaviour. In the present work, three different concentrations (0.1, 1.0 and 5.0 M) were used. Beside the above-mentioned dependencies, also a concentration influence could be observed. For low-concentrated electrolytes (0.1 M), there was a higher dissolution voltage E_{diss} than for the concentrated ones (1.0 and 5.0 M). Between the 1.0 and the 5.0 M electrolyte, there is almost no difference in E_{diss} but there is a distinct difference in the maximum of current density. So for higher concentrations, a higher current density and therefore a higher machining rate were observed. An overview about the dissolved alloy masses is given in Table 5. Figures 11 and 12 show the sample surfaces and side view, respectively.

A possible explanation for the differences between each electrolyte concentration might be the degree of coverage with the reactive ion species. For low concentrations (0.1 M), lower degrees of coverage can be assumed. In the case of Ti90Al6V4 in a NaCl electrolyte, pitting can be observed. This effect may result from a strong chemical interaction between the oxide surface and the halide ions which depends on the halide concentration, the layer thickness, the crystallinity and the applied voltage [25].

A higher voltage has to be applied to initiate a significant transpassive dissolution process. If the concentration of the reactive species increases (1.0 M), also the degree of coverage increases and the voltage for transpassive dissolution decreases. A further increase of electrolyte concentration does not lower the dissolution voltage E_{diss}, but it increases the conductivity of the electrolyte. The resulting current density is related to the conductivity of the electrolyte by the Ohm's law, and therefore, a higher conductivity leads to higher resulting current densities.

Using Faraday's law [26], it can be seen that a higher current density increases the dissolution rate of the material. So a higher concentration improves the machinability of an electrolyte system. The literature reports about an influence of electrolyte's flow rate on the removal behaviour of other materials like steel and cast iron [27, 28].

Table 5 Dissolved mass in macro-flow cell experiments for different alloys and electrolytes during a time period of 480 s

Alloy	Electrolyte	Dissolved mass
Ti90Al6V4	0.1 M $NaNO_3$	0.00384 g
Ti90Al6V4	0.1 M NaCl	0.00840 g
Ti90Al6V4	1.0 M $NaNO_3$	0.00407 g
Ti90Al6V4	1.0 M NaCl	0.12650 g
Ti90Al6V4	5.0 M $NaNO_3$	0.00443 g
Ti90Al6V4	5.0 M NaCl	0.22811 g
Ti60Al40	0.1 M $NaNO_3$	0.15105 g
Ti60Al40	0.1 M NaCl	0.17006 g
Ti60Al40	1.0 M $NaNO_3$	0.22878 g
Ti60Al40	1.0 M NaCl	0.30900 g
Ti60Al40	5.0 M $NaNO_3$	0.53946 g
Ti60Al40	5.0 M NaCl	0.67565 g

The influence of the flow rate on the removal behaviour was measured for Ti90Al6V4 in sodium chloride electrolyte. Flow rates of 0.35 and 0.6 L min^{-1} were used. The results show that the dissolution voltage E_{diss} was changed only around 100 mV. For higher flow rates, the dissolution starts earlier. During the dissolution process, gas evolution could not be avoided and for this reason, a higher flow rate is required to flush out the dissolution products and especially evolving gases. If the flow rate is too low, there is an accumulation of gas bubble in the gap between working and counter electrode and no reproducible results can be obtained due to a jumping current density signal.

A sufficient electrolyte flushing was reached at 0.6 L min^{-1}, and for this reason, the electrolyte flow rate kept constant for all experiments.

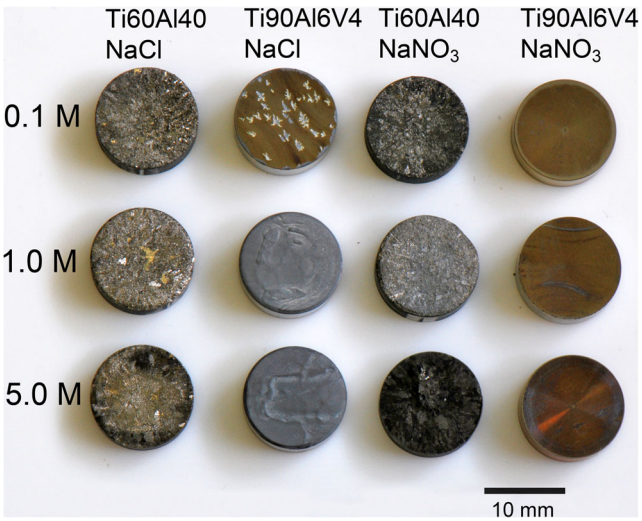

Fig. 11 Top view of the samples after ECM-like experiments in a macro-flow cell using NaCl and $NaNO_3$ electrolytes with different concentrations. The diameter of the samples is 12.45 mm

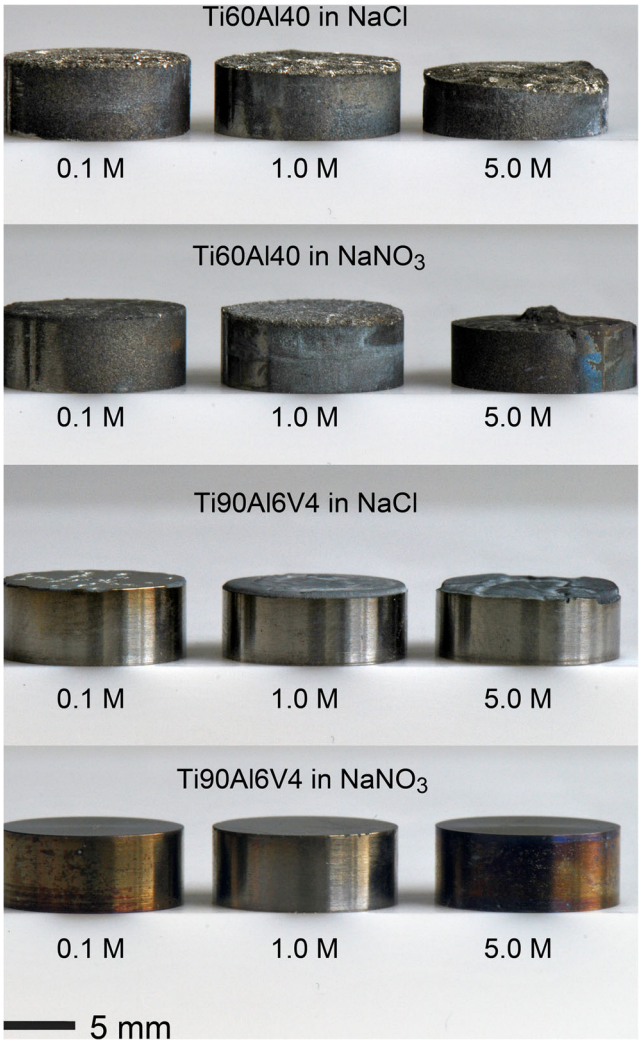

Fig. 12 Side view of the samples shows the influence of the different electrolytes on the dissolution rate in macro-flow cell experiments

For a better understanding of the dissolution process itself and the influence of the alloying elements, the ratio of dissolved ions in the used electrolyte is investigated by ICP-OES. For this series of experiments, during each chronoamperomeric measurement, a sample was taken from the electrolyte every minute and the titanium and aluminium content was determined. The development of the concentration ratio of aluminium and titanium is shown in Fig. 13. For each time step, the reproducibility was tested with four individual samples. The average value and the standard deviation are also shown.

Over the complete measuring period, a nearly constant ratio of Al/Ti ion concentrations can be observed. For the Ti60Al40 alloy, the measured concentrations fit with the expected ones. If the kinetic of the dissolution process for Ti and Al is comparable, there should be a ratio of 66 %. Our experiment shows a ratio between 56 and 70 %. The dissolution of Ti90Al6V4 shows a similar behaviour for the chloride containing electrolyte. The ratio of dissolved ions is also in the

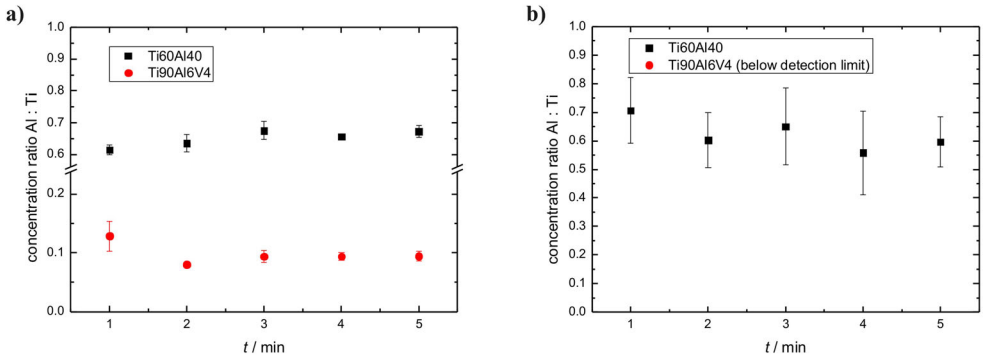

Fig. 13 Concentration of titanium and aluminium ions in the electrolyte after dissolution of Ti60Al40 (*black squares*) and Ti90Al6V4 (*red points*) in **a** 1 M NaCl and **b** 1 M $NaNO_3$ solution. For experiments of Ti90Al6V4 in nitrate electrolytes, the concentrations of Ti and Al ions are below the detection limit and are not displayed. The *error bars* resulting from the standard deviation

expected range of about 7 % and almost constant for the whole period. In the case of measuring Ti90Al6V4 in a nitrate electrolyte, the amount of dissolved ions was below the detection limit of the ICP-OES analysis. Therefore, no results are shown. The error bars in Fig. 13b are bigger than in Fig. 13a because the dissolved mass of the sample is very low and therefore, the errors of the analysis increase also. So we assume for both electrolytes that there is no favoured dissolution of one element because titanium and aluminium are dissolved in comparable amounts.

Conclusions

1. A Ti60Al40-alloy was prepared by arc melting. The resulting samples are chemically and structurally homogeneous. A tetragonal crystal structure can be determined by Rietveld refinement.
2. The existence of a natural oxide layer on top of Ti90Al6V4 and Ti60Al40 was verified by EIS. Comparing the measurements with the model of González et al., the oxide layer of Ti60Al40 is less distinct than the oxide layer of Ti90Al6V4.
3. The evolution of the oxide layer depends on the type of electrolyte, on the pre-treatment of the alloy and on the alloy composition:
   - The oxidation power of the used electrolyte anions increases in the order $Cl^- < NO_3^- < ClO_3^-$ shifting E_{OCP} to more positive values due to enhanced oxide layer formation.
   - Comparing an etched, a natural and an oxidized surface, the shift of E_{OCP} to more positive values is caused by an increased oxide layer.
   - E_{OCP} for Ti90Al60V4 is more positive than for Ti60Al40 because the titanium content of the alloy leads to a higher oxidation.
4. The dissolution of the alloys in flow cell measurements was influenced by the type of alloy and electrolyte, the electrolyte concentration and flow rate:
   - Compared with Ti60Al40, E_{diss} of Ti90Al6V4 is increased because of the distinction of the oxide layer. Non-halide containing electrolytes lead for Ti90Al6V4 to passivation whereas Ti60Al40 can be dissolved in non-halide and halide containing electrolytes.
   - Effective electrolytes for the dissolution of titanium alloys contain halides. The reason for this could be a two-step mechanism which was proposed by the literature.
   - The concentration of the electrolyte influences E_{diss} and the resulting current density. For concentrations above 1 M, the influence of the electrolyte concentration decreases, whereas the current density increases with the electrolyte concentration due to a higher conductivity.
   - E_{diss} is marginal influenced by the electrolyte flow rate. A minimum flow rate of 0.6 L min^{-1} is necessary to remove reaction products and gas bubbles from the electrode surface.
5. The homogeneous dissolution of the alloying elements was verified by time-resolved ICP-OES analysis.

Summarizing the present results, both titanium alloys are suitable for ECM applications but the electrolytes and the applied potentials have a large influence on the machining behaviour. Depending on the alloy and the desired structure, the experimental parameters have to be carefully chosen. For industrial processes, it is very difficult to optimize a set of parameter in a running production plant. For this reason, preliminary studies are necessary. As shown in the present study, these kinds of experiments (micro- and macro-flow cell) are a powerful tool to determine a set of appropriate machining parameter.

Acknowledgments This work was financially supported by the European Union within the Interreg IV A programme "Initiative PRECISE". We thank Prof. Dr. Rolf Hempelmann and Prof. Dr.-Ing. Dirk Bähre for fruitful discussions and Elfi Jungblut, Dipl.-Ing. Sylvia Kuhn, M. Sc. Dan Durneata, Andreas Kirsch and Dr. Nathalie Kunkel for the experimental support.

References

1. Long M, Rack HJ (1998) Biomaterials 19:1621–1639
2. Rack HJ, Qazi JI (2006) Mater Sci Eng C 26:1269–1277
3. Wang K (1996) Mater Sci Eng A 213:134–137
4. Peters M, Kumpfert J, Ward C, Leyens C (2003) Adv Eng Mater 5: 419–427
5. Boyer RR (1996) Mater Sci Eng A 213:103–114
6. Niinomi M (1998) Mater Sci Eng A 213:231–236
7. Froes FH, Suryanarayana C, Eliezer D (1992) J Mater Sci 27:5113–5140
8. Aspinwall DK, Dewes RC, Mantle AL (2005) CIRP Manuf Technol 54:99–104
9. Bhattacharyya B, Mitra S, Boro AK (2002) Robot CIM-INT Manuf 18:283–289
10. van Noort R (1987) J Mater Sci 22:3801–3811
11. de Assis SL, Wolynec S, Costa I (2006) Electrochim Acta 51:1815–1819
12. González JEG, Mirza-Rosca JC (1999) J Electroanal Chem 471:109–115
13. Lohrengel MM, Rosenkranz C, Klüppel I, Moehring A, Bettermann H, Van den Bossche B, Deconinck J (2004) Electrochim Acta 49: 2863–2870
14. Eppelsheimer D, Perman R (1950) Nature 166:960
15. Downs RT, Bartelmehs KL, Gibbs GV, Boisen MB (1993) Am Mineral 78:1104–1107
16. Murray JL (1988) Metall Trans A 19:243–247
17. Schenk R (2001) The corrosion properties of titanium and titanium alloys. In: Brunette DM, Tengvall P, Textor M, Thomsen P (eds) Titanium in Medicine. Springer, Berlin Heidelberg, pp 145–170
18. Pan J, Thierry D, Leygraf C (1996) Electrochim Acta 41:1143–1153
19. Tomashov ND, Chernova GP, Ruscol YS, Ayuyan GA (1974) Electrochim Acta 9:159–172
20. Hefny MM, Mazhar AA, El Basiouny MS (1982) Br Corros J 17:38–41
21. El Basiouny MS, Mazhar AA (1982) Corrosion 38:237–240
22. Hirschorn B, Orazem ME, Tribollet B, Vivier V, Frateur I, Musian M (2010) J Electrochem Soc 157:C452–C457
23. Bannard J (1976) J Appl Electrochem 6:477–483
24. Rolsten RF (1968) J Appl Chem 18:292–296
25. Casillas N, Charlebois SJ, Smyrl WH, White HS (1993) J Electrochem Soc 140:L142–L145
26. Faraday M (1834) Philos Trans R Soc 124:77–122
27. Da Silva Neto JC (2009) Proceedings of COBEM 2009
28. Wang S, Zeng Y, Liu Y, Zhu D (2012) Int J Adv Manuf Technol 63: 25–32